BIOCHEMISTRY
including biophysical chemistry & molecular biology

Article

pubs.acs.org/biochemistry

Base Pair Opening in a Deoxynucleotide Duplex Containing a *cis-syn* Thymine Cyclobutane Dimer Lesion

Belinda B. Wenke,[§] Leah N. Huiting,[§] Elisa B. Frankel,[§] Benjamin F. Lane,[‡] and Megan E. Núñez*[,§,†]

[§]Department of Chemistry, Mount Holyoke College, South Hadley, Massachusetts 01075, United States

[‡]Charles Stark Draper Laboratory, Cambridge, Massachusetts 02139, United States

[†]Department of Chemistry, Wellesley College, Wellesley, Massachusetts 02481, United States

Supporting Information

ABSTRACT: The *cis-syn* thymine cyclobutane dimer is a DNA photoproduct implicated in skin cancer. We compared the stability of individual base pairs in thymine dimer-containing duplexes to undamaged parent 10-mer duplexes. UV melting thermodynamic measurements, CD spectroscopy, and 2D NOESY NMR spectroscopy confirm that the thymine dimer lesion is locally and moderately destabilizing within an overall B-form duplex conformation. We measured the rates of exchange of individual imino protons by NMR using magnetization transfer from water and determined the equilibrium constant for the opening of each base pair K_{op}. In the normal duplex K_{op} decreases from the frayed ends of the duplex toward the center, such that the central TA pair is the most stable with a K_{op} of 8×10^{-7}. In contrast, base pair opening at the 5′T of the thymine dimer is facile. The 5′T of the dimer has the largest equilibrium constant ($K_{op} = 3 \times 10^{-4}$) in its duplex, considerably larger than even the frayed penultimate base pairs. Notably, base pairing by the 3′T of the dimer is much more stable than by the 5′T, indicating that the predominant opening mechanism for the thymine dimer lesion is not likely to be flipping out into solution as a single unit. The dimer asymmetrically affects the stability of the duplex in its vicinity, destabilizing base pairing on its 5′ side more than on the 3′ side. The striking differences in base pair opening between parent and dimer duplexes occur independently of the duplex-single strand melting transitions.

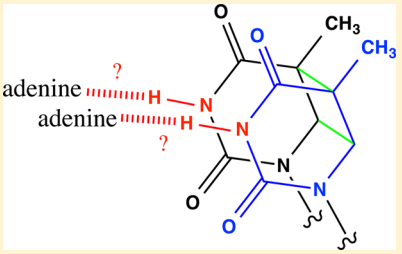

Genomic DNA is constantly under attack by a variety of exogenous and endogenous agents that covalently modify its structure.[1] These covalent modifications must be repaired lest they lead to mutations, cancer, and cell death. One of the most thoroughly studied DNA lesions is the *cis-syn* thymine cyclobutane dimer lesion. One of a family of pyrimidine photoproducts, the thymine dimer lesion is formed by a UV light-promoted [2 + 2] cycloaddition reaction between two adjacent thymines, resulting in the formation of a permanent cyclobutane ring between the 5,6-positions. The thymine dimer stalls replicative and transcriptional polymerases,[2−4] leading to bypass replication by error prone polymerases such as pol η in the former case,[5,6] and to transcription coupled repair in the latter.[7,8] In the absence of efficient repair, the thymine dimer can lead to mutations, cancer, or cell death.

The structure of the *cis-syn* thymine cyclobutane dimer lesion has been studied for more than forty years, first in UV-irradiated mixed-sequence genomic DNA or as a dinucleobase model, and later by NMR and X-ray crystallography in synthetic oligodeoxynucleotide duplexes. Circularization and electrophoretic mobility assays indicated that this lesion bends the DNA by between 7° and 30°.[9,10] The crystal structure revealed a DNA duplex that was largely B-form, but with a bend toward the major groove of ∼30° and an unwinding of approximately 9° localized to the three base pairs around the lesion.[11] Hydrogen bonding of the 3′ thymine of the dimer appeared relatively normal, while the hydrogen bonding on the 5′ thymine was longer and weaker than normal. The NMR solution structure of the thymine dimer similarly showed a predominantly B-form duplex, but with a smaller bending angle (∼7°) and a small overwinding of the helix.[12] Again, the hydrogen bonding of the thymine dimer appeared strong at the 3′ thymine but weak at the 5′ thymine of the dimer.

Like many repair proteins, both the direct-photoreversal catalyst photolyase and the excision repair enzyme T4 endonuclease V utilize base flipping to facilitate access to the thymine dimer lesion.[13−15] Co-crystal structures of the thymine dimer lesion with these proteins illustrated an interesting anomaly: photolyase induces a 50° bend in the DNA and flips the lesion into its active site, while the endonuclease flips out the adenine paired with the 5′ thymine, causing the DNA to bend in the *opposite* direction. Recent computational studies support the idea that the barrier to base flipping at the lesion site might be low,[16] and thermodynamic studies suggest that photolyase might bind an already extruded lesion.[17]

In aggregate, these results led us to wonder whether the DNA at the thymine dimer lesion site is naturally bendable due to innate weakening of base pairs at the lesion site, and whether base pair opening at the lesion site occurs spontaneously or is facilitated by repair proteins. To examine the stability and

Received: September 20, 2013
Revised: November 27, 2013
Published: December 11, 2013

   dx.doi.org/10.1021/bi401312r | *Biochemistry* 2013, 52, 9275−9285

dynamics of the base pairs at and around the thymine dimer lesion, we used NMR imino exchange measurements to measure the base pair equilibrium constants for each thymine in the thymine dimer lesion and its flanking bases.

METHODS AND MATERIALS

Preparation of DNA Samples. DNA oligonucleotides were prepared commercially via automated phosphoramidite synthesis (Midland Certified Reagent Company, Integrated DNA Technologies) using the thymine dimer phosphoramidite. Each strand was purified by HPLC after deprotection, and its integrity was confirmed by mass spectrometry. Oligonucleotides were then desalted in C18 cartridges (Sep-Pak, Waters Corp.) and dialyzed extensively against 1× NMR Buffer (10 mM sodium phosphate pH 7.5, 5 mM NaCl), followed by Exchange Buffer (40 mM ammonium chloride buffer pH 8.2, 50 mM NaCl) where applicable. Oligonucleotide concentrations were determined spectrophotometrically using the following molar extinction coefficients: ε_{260} = 95 200 for strand 3, ε_{260} = 77 000 for strand 3TT, and ε_{260} = 104 000 for strand 4. Samples were prepared by mixing equimolar amounts of each strand in phosphate or ammonium buffer, heating to 90 °C, and cooling slowly to 8 °C to allow for annealing. DNA samples for NMR were prepared to the following initial duplex concentrations, maximized to the yield of available single strands: Parent NOESY sample: 800 μM; Dimer NOESY sample: 440 μM; Parent titration #2: 800 μM; Parent titration #3: 500 μM, Dimer titration #1: 600 μM, Dimer titration #2: 500 μM. When not in use, NMR samples were stored at 8 °C in a commercially available wine refrigerator. D_2O was added to the NMR samples to a final concentration of 5% for the NMR lock.

4 M stock solutions of the ammonium chloride catalyst were prepared at pH 8.2 and small aliquots were added directly to the NMR tube to achieve the desired catalyst concentration. Estimating the pK_a to be 9.3 at 8 °C, the fraction of active ammonia is 1/13.75 of the total ammonium species in solution.

Circular Dichroism Spectropolarimetry. CD spectra were measured at 10 °C on a Jasco J-715 spectropolarimeter using a 0.1 cm cuvette. DNA samples were prepared at an 8 μM concentration of each strand. Spectra were collected at 0.2 nm increments between 320 and 220 nm with a scanning rate of 20 nm/min. The buffer blank was subtracted from each spectrum, a correction was applied for the nucleotide concentration and path length, and the spectra were normalized to units of molar ellipticity, resulting in the final spectra shown here.

UV Melting Thermodynamic Studies. DNA duplexes were prepared to concentrations between 1.5 and 21 μM in 10× NMR buffer (100 mM sodium phosphate pH 7.5, 50 mM NaCl), annealed by heating and gradual cooling, and degasssed at 4 °C. Samples were placed in matched quartz cuvettes (0.1 cm, 0.2 cm, 0.5 cm, or 1 cm), and the absorbance at 260 nm was measured on a Varian Cary 50 UV−visible spectrophotometer with a Peltier temperature-controlled cell. The absorbance was measured every 0.1 min while ramping the temperature upward at 1.0 °C/min from 8 to 80 °C. The inflection point on the temperature vs absorbance curve was determined from the first derivative. At least six independent measurements were made at each of the five duplex concentrations.

The T_m values and concentrations were used to determine the entropy and enthalpy changes for the duplex-single strand equilibrium using the van't Hoff equation. A plot of $1/T_m$ versus ln C_{tot} is a straight line whose slope and intercept relate to the change in enthalpy and entropy associated with duplex formation

$$\frac{1}{T_m} = \frac{R(\ln C_{tot})}{\Delta H} + \frac{(\Delta S - 1.39R)}{\Delta H} \quad (1)$$

where C_{tot} is the total concentration of DNA strands, i.e., twice the duplex concentration. The change in Gibbs free energy associated with duplex formation was calculated from ΔH and ΔS at 25 °C.

1D ^{1}H and 2D NOESY NMR Spectra. 1D ^{1}H NMR spectra were obtained at Mount Holyoke College on a Bruker AVANCE 400 MHz equipped with a broadband inverse (BBI) probe. Water suppression was achieved using a 3−9−19 pulse sequence with gradients. 1D spectra were recorded at 8 °C both in 1× NMR buffer with no added catalyst and in Exchange Buffer with 40 mM catalyst. The spectra were nearly identical regardless of buffer, so the latter are shown here. DSS was used to calibrate the chemical shift axis.

2D NOESY spectra were obtained at Smith College on a Bruker AVANCE 500 MHz equipped with a multinuclear broadband Fluorine observe SmartProbe. Two spectra were obtained for each sample, one in 5% D_2O/95% H_2O, and the other in 100% D_2O (Cambridge Isotope Laboratory). In the first case, the spectral dimensions were 20 ppm (^{1}H, 2048 complex points) by 20 ppm (^{1}H, 512 complex points). 64 scans were accumulated with a recycling delay of 1.5 s and a mixing time of 250 ms. Water suppression was achieved via a Watergate W5 sequence. In the second case, the spectral dimensions were 22 ppm (^{1}H, 2048 complex points) by 22 ppm (^{1}H, 512 complex points). Forty scans were accumulated with a recycling delay of 8 s and a mixing time of 150 ms. Spectra were superimposed, their resonances assigned, and their chemical shifts measured in Sparky[18] according to the NOE walk method.[19−21] In the absence of COSY experiments, H4′ and H5′ protons were not assigned. A model of parent duplex **3**−**4** was created using Nucleic Acid Builder written by the Case group at Rutgers University.[22] The model was utilized in iMol without further refinement purely for visualization.

Measurement of Base Pair Opening by NMR. We used magnetization transfer from water protons as described by Guéron and Leroy[23] to measure the base pair opening equilibrium via exchange of the imino protons on guanine and thymine. Having previously described at some length how we utilize these experiments,[24] we will describe here only a few relevant details.

These experiments were performed on a Bruker AVANCE 400 MHz NMR using a BBI probe at Mount Holyoke College. Inversion of water proton magnetization utilized a DANTE pulse scheme, magnetization transfer occurred during a variable mixing time (t_{mix}), and a jump-and-return sequence was used to suppress the water peak. Gradients were used to suppress components of transverse solvent magnetization and reduce radiation damping. Spectra were measured at 8 °C, as determined by calibration to a methanol reference standard.[25]

The critical parameters for water inversion, i.e., the efficiency of water inversion E and the longitudinal relaxation rate for water R_{1w} were determined as described previously for each experimental sample at every ammonia concentration.[24] Imino exchange rates were determined at 24 mixing times between 520 μs and 2.5 s. The NMRPipe suite of programs[26] was used to uniformly zero fill, Fourier transform, phase, crop, and apply

dx.doi.org/10.1021/bi401312r | Biochemistry 2013, 52, 9275−9285

a first order baseline to each group of 24 spectra, as well as to establish the approximate chemical shift of each peak. Exchange and relaxation times were determined in Matlab (MathWorks, Natick MA) as follows: the exchange rate for each imino peak (k_{ex}) was estimated by nonlinear least-squares fitting of the peak heights as a function of time to eq 2:

$$\frac{I_z(t_{mix})}{I_{z,eq}} = 1 + E \times k_{ex} \times (e^{-R_{1i}t_{mix}} - e^{-R_{1w}t_{mix}}) \quad (2)$$

E and R_{1w} were determined as described above, and $I_z(t_{mix})$ and $I_{z,eq}$ were the measured intensities of the imino peaks after time t_{mix} or at equilibrium. The exchange rate k_{ex} and R_{1i} (which represents a combination of the imino proton relaxation rate and the chemical exchange rate k_{ex}) were determined by fitting eq 2 to the data.

At very low catalyst concentrations similar to those used here, the apparent equilibrium constant for base pair opening αK_{op} and the intrinsic rate of exchange k_{int} can be determined from a plot of the k_{ex} versus [B] according to the following simplified linear relationship as described by Every and Russu:[27]

$$k_{ex} = \alpha K_{op}(k_{int} + k_B[B]) \quad (3)$$

The exchange data measured between 2.9 mM and 29 mM ammonia catalyst were fit to this equation in Matlab to give best-fit values of k_{int} and αK_{op} together with their associated uncertainties. Guéron and colleagues measured α to be approximately equal to one for the ammonia base catalyst,[28] and thus it is excluded from the equation. k_B is a second-order rate constant for base catalysis, a constant that can be directly calculated for each type of imino proton

$$k_B = \frac{k_D}{(1 + 10^{pK_a^{nu} - pK_a^{B}})} \quad (4)$$

With a biomolecular collision rate k_D approximately equal to 1.0×10^9 M^{-1} s^{-1}, the k_B of DNA nucleotides in ammonia buffer was calculated to be 2.0×10^8 M^{-1} s^{-1} for thymine, 3.9×10^8 M^{-1} s^{-1} for guanine, and 3.8×10^7 M^{-1} s^{-1} for the thymine dimer protons. These calculations are based on approximate pK_a values at 8 °C of 9.3 for ammonia, 9.9 for thymidine, 9.5 for guanosine, and 10.7 for both thymine dimer protons;[23,29] other values of k_B are obtained with higher thymine dimer pK_a estimates.

RESULTS

In this study, we set out to explore the base pairing stability of DNA containing a *cis-syn* thymine dimer lesion. The 10-base pair DNA oligonucleotide duplexes used in this study are shown in Table 1. Duplex **3**−**4** (the control parent duplex) and Duplex **3TT-4** (the duplex containing the *cis-syn* thymine cyclobutane dimer lesion) are identical except for the presence of the lesion at thymines 5 and 6. This non-palindromic sequence, which displayed the best dispersion of the imino peaks in the ^{1}H NMR spectrum among all of the duplexes we screened, was first studied twenty years ago by J.-S. Taylor and colleagues.[30]

UV Melting Thermodynamics and Circular Dichroism Spectropolarimetry. UV melting thermodynamic measurements and circular dichroism spectropolarimetry were used to assess the global stability and structure of the duplex containing the thymine dimer. A series of parent and dimer duplex samples was prepared at a range of concentrations between 28 and 1.5 μM. In all cases, the absorbance at 260 nm increased during heating via a classic single, sharp transition between 15° and 30 °C, characteristic of a cooperative two-state transition between dsDNA and ssDNA (SI Figure 1). The melting temperature (T_m), taken as the inflection point of the melting curve, was lower for the dimer sample than the parent sample at all concentrations. A plot of the $1/T_m$ versus the natural log of the concentration illustrates the loss in duplex stability due to the duplex (Figure 1A). The thermodynamic parameters ΔH and ΔS were obtained by linear fits of the van't Hoff equation (eq 1) to Figure 1A, and these were used to determine the Gibbs free energy for duplex formation (Figure 1B). In this sequence, the presence of the thymine dimer lesion increases the enthalpic stability of the duplex but decreases the entropic instability, leading to an overall small loss in free energy of +1.5 ± 0.1 kcal/mol (SI Table 1).

Table 1. Sequences of the 10 bp DNA Oligonucleotide Duplexes.[a]

Parent Duplex ***3-4***

Strand 3	5'- C_1 G_2 T_3 A_4 **T_5** **T_6** A_7 **T_8** G_9 C_{10} -3'
Strand 4	3'- G_{20} C_{19} A_{18} T_{17} A_{16} A_{15} T_{14} A_{13} C_{12} G_{11} -5'

Lesion Duplex ***3TT-4***

Strand 3TT	5'- C_1 G_2 T_3 A_4 **T_5<>T_6** A_7 **T_8** G_9 C_{10} -3'
Strand 4	3'- G_{20} C_{19} A_{18} T_{17} A_{16} A_{15} T_{14} A_{13} C_{12} G_{11} -5'

[a]Nucleotides are numbered sequentially from the 5′ end of each strand, indicated with subscripts. Location of the thymine cyclobutane dimer lesion, at thymines 5 and 6, is designated by T<>T.

The circular dichroism spectrum of the parent duplex displays a maximum around 279 nm, a crossover at 266 nm, a minimum around 248 nm, and another maximum around 220 nm, consistent with a B-form duplex (Figure 1C). Notably, the spectra of the parent and dimer oligonucleotides, in both the double- and single-stranded forms, show pronounced differences. The positive band observed in the parent spectrum around 280 nm is larger in magnitude and shifted to shorter wavelengths in the dimer duplex, whereas the negative band around 248 nm in the parent spectrum occurs at the same wavelength in the dimer but is smaller in magnitude. In contrast, the positive band at 280 nm in the single-stranded parent sample is diminished in the dimer sample and shifts to higher wavelength; the magnitude of the band around 250 nm decreases only modestly, and occurs at the same wavelength in parent and dimer. In making pairwise comparisons, one can also notice that the dimer spectra change more dramatically between the single-stranded form and the double-stranded form than do the parent spectra.

Assignment of Exchangeable Protons by 2D NOESY NMR Spectroscopy. We used the thymine and guanine base imino protons as handles to explore the base pairing stability in lesion and control duplexes. To assign the imino proton resonances in the 1D ^{1}H NMR spectra (Figure 2), we obtained 2D NOESY spectra of parent and dimer duplexes in both 95% H_2O/5%D_2O and 100% H_2O. We assigned the nonexchangeable aromatic protons, H1′ sugar protons, and thymine methyl protons using NOE walk connectivities, independently generating assignments consistent with those of J.-S. Taylor and colleagues (SI Scheme 1, SI Figures 2−7, SI Tables 2−3).[30] Unlike the previous study of this sequence, we also assigned the exchangeable imino protons (Figure 2). The imino protons can

dx.doi.org/10.1021/bi401312r | *Biochemistry* 2013, 52, 9275−9285

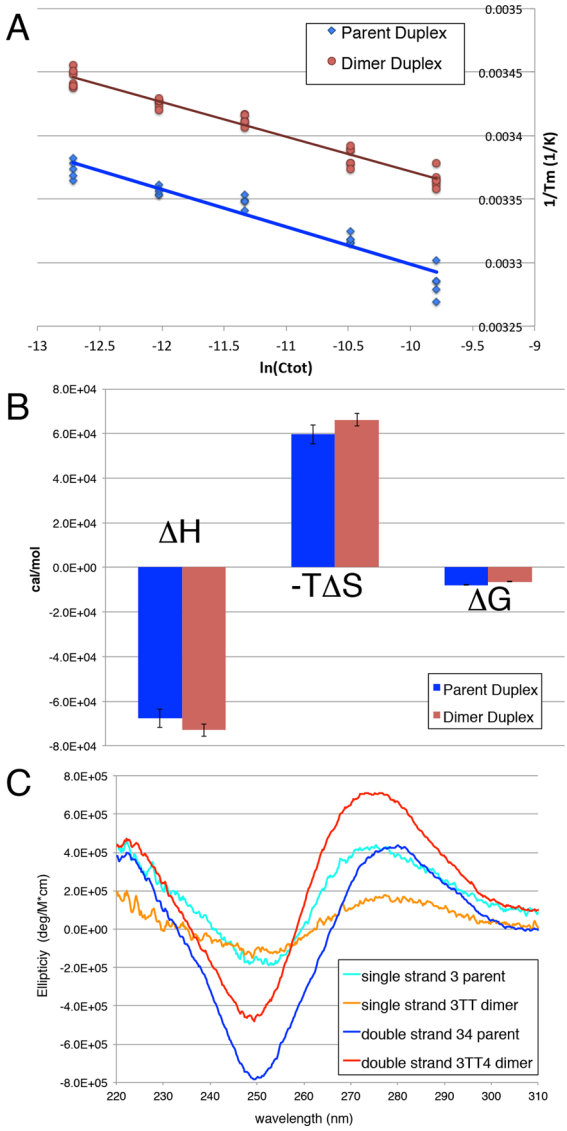

Figure 1. UV melting thermodynamics and circular dichroism (CD) spectra. (A) van't Hoff analysis of changes in melting temperature (T_m) as a function of duplex concentration for parent (blue diamonds, bottom line) and dimer (red circles, top line) duplexes. Changes in the UV absorption at 260 nm were measured in 10× NMR buffer, and the T_m was determined to be the inflection point in the melting curves. Six or more samples were measured for each concentration, and data were fit to eq 1 to determine the changes in enthalpy and entropy for duplex formation. (B) Thermodynamic parameters for duplex formation for parent (blue) and dimer (red) duplexes. A gain in enthalpic stability with dimer formation is counterbalanced by a gain in entropic instability, leading to an overall change in free energy $\Delta\Delta G$ of +1.5 kcal/mol. (C) CD spectra of single-strand 3 (cyan), dimer-containing strand 3TT (orange), parent duplex 3−4 (blue), and dimer duplex 3TT-4 (red), plotted as ellipticity in degrees/cm*M base pairs.

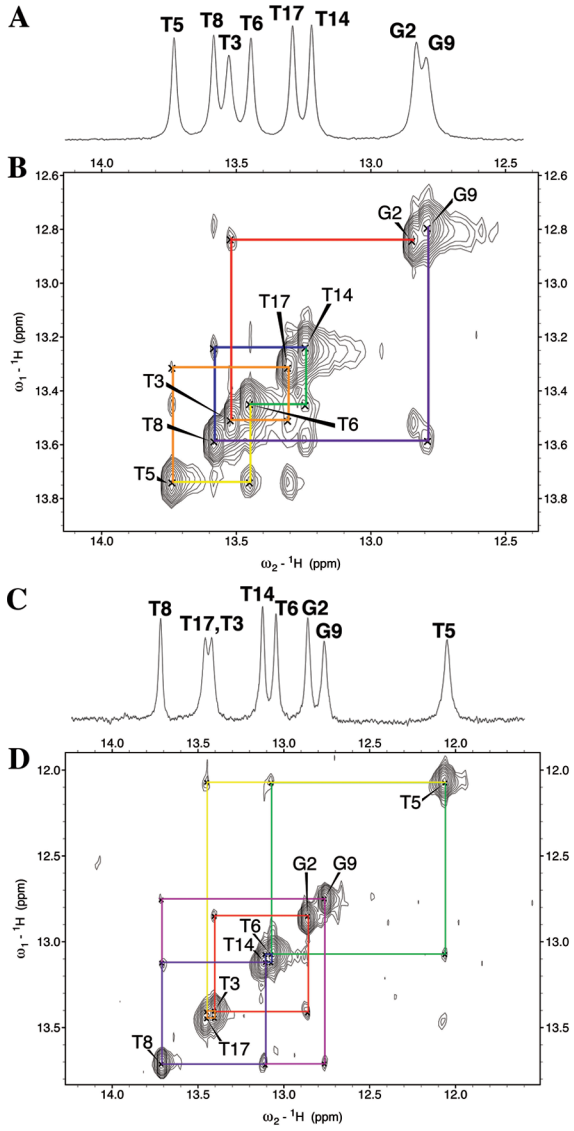

Figure 2. Imino proton resonances in the ^{1}H NMR spectra. (A) 1D ^{1}H spectrum of the parent duplex **3**−**4**, measured in Exchange Buffer at 40 mM total ammonia species. Assignments are based on the 2D NOESY spectrum immediately below. (B) Imino-imino region of the 2D NOESY spectrum for parent duplex **3**−**4**, measured in 1× NMR buffer. The NOE walk through the crosspeaks shows the connections between adjacent thymine and guanine imino protons in the core of the duplex. The chain can be traced from G_2 to G_9; the terminal guanines G_{11} and G_{20} are not seen here. (C) 1D ^{1}H spectrum of the dimer duplex 3TT-4, measured in Exchange Buffer at 40 mM total ammonia species. (D) Imino-imino region of the 2D NOESY spectrum for dimer duplex 3TT-4, measured in 1× NMR buffer. Note that the imino proton resonance for the 5′ thymine of the thymine dimer, T_5, shifts markedly upfield from its position in the parent duplex; that of the 3′ thymine T_6 moves more modestly.

generally be assigned by an NOE walk along the center of the duplex; however, in this case, the DNA is pseudo-palindromic in that the sequence of *imino* protons (i.e., GGTTTTTTGG) is identical from either end of the duplex. The orientation of the duplex was confirmed by NOE connectivities from the guanine iminos to paired cytosine N4 protons, which are in turn connected to the cytosine C5 and C6 protons (SI Figures 8−11).

In both duplexes, the thymine imino protons are found far downfield around 13−14 ppm relative to DSS in a region of the spectrum otherwise empty of DNA proton resonances, and the guanine imino protons slightly less downfield around 12.8 ppm (Figure 2). The two penultimate guanines, G_2 and G_9, are sharp and reasonably well-resolved, but the terminal guanines, G_{11} and G_{20}, appear as a single short, broad peak at 8 °C, and disappear entirely in the presence of catalyst. In the dimer duplex, the imino proton resonance for the 5′ thymine of the

dx.doi.org/10.1021/bi401312r | *Biochemistry* 2013, 52, 9275−9285

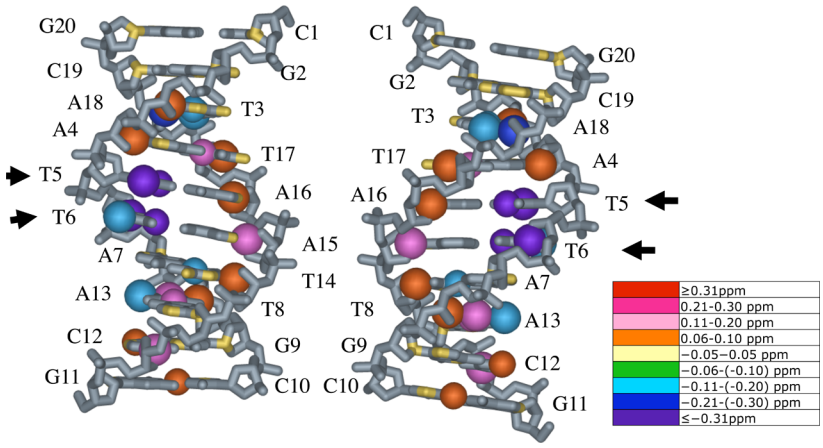

Figure 3. Chemical shift differences between parent and dimer duplex NOESY spectra. The model of parent duplex **3**−**4** is shown from the minor and major grooves. Each diagram is color-coded as indicated in the legend to illustrate the magnitude in the differences in proton chemical shift between parent and dimer duplex. Wireframe structures in the default gray color indicate that the protons were not assigned (i.e., the H4′ and H5′ protons), and pale yellow wireframes indicate that the magnitude of the chemical shift change was less than ±0.05 ppm. Protons represented by colored spheres experience a chemical shift change greater than ±0.05 ppm. Arrows indicate the position of the thymine dimer lesion in the dimer duplex. Annotated NOESY spectra and tabulated values of the chemical shifts are given in the Supporting Information.

thymine dimer (T_5) is shifted upfield substantially to ∼12.05 ppm, a change of more than 1.6 ppm. In contrast, the 3′ thymine (T_6) resonance is shifted more subtly upfield by almost 0.4 ppm.

To compare all of the assigned protons in the parent duplex to those in the dimer duplex, we then mapped the changes in chemical shift between the two duplexes onto a simple, color-coded molecular model of the parent duplex (Figure 3). Though this diagram represents only a map of chemical shift changes and not an optimized structure, it allows us to see at a glance where the greatest disturbances in duplex structure and electronics occur. Not surprisingly, the nucleotides that experience the largest upfield perturbations in chemical shift are those that form the thymine dimer itself, consistent with the loss of aromaticity in the dimer (Figure 3, violet spheres). More modest upfield (cyan, blue spheres) and downfield (orange, pink spheres) shifts are also observed scattered throughout the short duplex. This diagram highlights the changes in chemical shift of the H1′ protons along the complementary strand, illustrating that the dimer subtly alters the overall backbone shape of the duplex. However, the majority of the protons exhibit little or no difference in chemical shift (Δppm = 0.05 to −0.05, yellow wireframe) reflecting the similarity of the structure and electronic environment of both duplexes. The aromatic and H1′ protons on the terminal and penultimate C_1-G_{20} and G_2-C_{19} base pairs, 3−4 base pairs away, experience almost no change in chemical environment between duplexes.

Examining Base Pairing Using the Imino Protons. Based upon a two-state model for DNA melting and the UV melting thermodynamic data we estimated that the duplexes would melt around ∼38 °C for the parent duplex and ∼31 °C for the dimer duplex at the 500 μM duplex concentration used for most of our NMR experiments. To examine the melting process from the perspective of each base pair, we measured 1D spectra of both duplexes at 3°, 8°, 13°, 18°, 23°, and 28° (Figure 4). As would be expected, the resonances shift upfield and gradually become shorter and broader with increasing temperature. At 28 °C they disappear entirely from the dimer, but not the parent, spectrum. It is interesting to note that neither of the two dimer protons (at T_5 nor T_6) disappears or otherwise behaves differently than the other protons in their duplex, but surprisingly T_{17} (the base 3′ to T_5's complementary adenine) broadens and disappears at a lower temperature than any of the other internal bases.

These simple experiments give us only a qualitative sense of the structural integrity of the DNA around the lesion. To measure quantitatively the base pair opening dynamics at and around the thymine dimer lesion, we used magnetization transfer between solvent water protons and guanine and thymine imino protons.[23] Since the imino protons are normally locked up in hydrogen bonds at the center of the DNA base stack, they can only exchange with solvent when the base pairs are broken and one or both bases in the pair open to solvent. To observe the rapid exchange with solvent, we inverted the solvent water protons with a 90° pulse and then measured the height of the imino proton resonances after a variety of delay times between 520 μs and 2.5 s. As seen in Figure 5, the imino proton resonances get shorter as they exchange and then taller again as both the DNA and water protons relax. The protons that exchange the most rapidly and thoroughly with solvent (i.e., on the penultimate bases G_2 and G_9 and the 5′ T of the dimer T_5) are inverted, while those that exchange slowly remain positive.

We can use these data and eq 4 to determine the exchange rate k_{ex} of each imino proton individually. Unfortunately, the bases do not always exchange their imino protons with solvent every time the base pair is broken, so these values of k_{ex} underestimate the true opening rate of the base pairs. To abstract the imino protons we titrate increasing amounts of ammonia base as a catalyst and examine the imino exchange rate as the catalyst increases (Figure 6). Across the range of catalyst concentrations, the rates of imino proton exchange are significantly different between the parent and the dimer duplexes, with much faster exchange observed at some locations in the dimer duplex, but not all. In the parent duplex, only the penultimate bases G_2 and G_9 exchange at a rate above 50 s^{-1}, even at the highest concentrations of catalyst. These penultimate guanines exchange more quickly than the unmodified, interior thymines due to end fraying. In the dimer duplex, several of the imino protons exchange more rapidly than in the parent duplex, although notably not all of them. The penultimate bases G_2 and G_9 and the dimer proton

dx.doi.org/10.1021/bi401312r | *Biochemistry* 2013, 52, 9275−9285

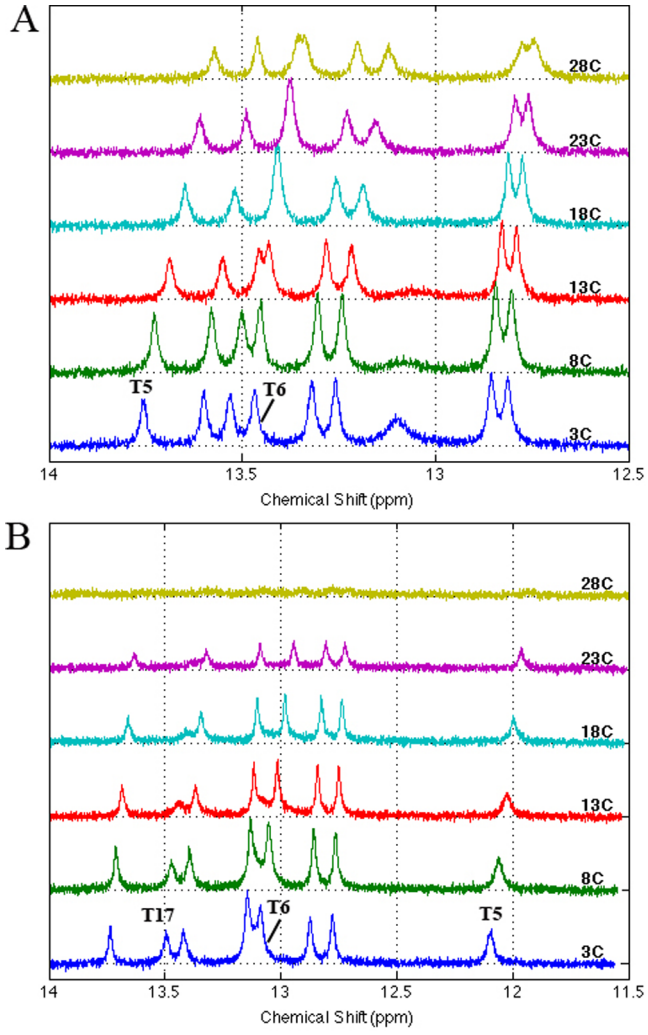

Figure 4. Imino proton resonances in the ^{1}H NMR spectra as a function of temperature. (A) For the parent duplex **3**–**4**, all of the imino peaks are visible to 28 °C in 1× NMR buffer, though some change in chemical shift and line broadening does occur as expected. (B) For dimer duplex **3TT-4**, the duplex melts cooperatively between 23° and 28 °C in 1× NMR buffer. Both dimer imino protons, T_5 and T_6, are visible below this range. Note that the ammonia-catalyzed imino proton exchange experiments are performed at 8 °C.

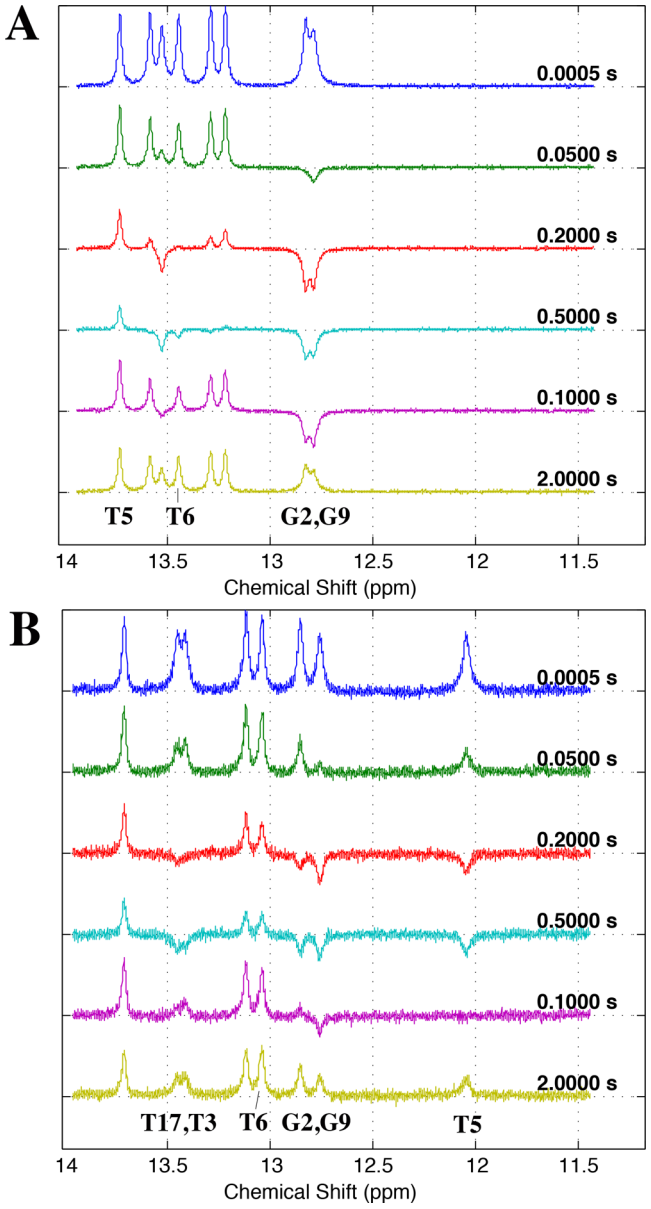

Figure 5. Imino proton exchange via magnetization transfer from water. The water protons are inverted via a 90° pulse, and the 1D spectrum of the imino protons is obtained after a range of 24 delay times between 520 μs and 2.5 s. Parent (A) and dimer (B) duplex spectra are shown here at five representative delay times at 2.9 mM ammonia base catalyst. These spectra illustrate how the resonances shrink or invert, then slowly return to equilibrium as the water and imino protons relax. At higher catalyst concentrations, proton exchange is more efficient and thus inversion of the resonances is more complete. The exchange rate of the imino protons (k_{ex}) is determined from plots of the amplitude of each peak as a function of time, as fit to eq 2.

on T_5 exchange the most quickly, becoming too fast to measure once they exceed 250 s^{-1}. The thymine imino protons on the half of the duplex that is 5′ to the dimer, T_{17}/T_3 (poorly resolved in the dimer, and thus representing an average value), exchange more quickly than either the corresponding parent protons or the imino protons on the half of the duplex that is 3′ to the dimer. In contrast, the k_{ex} values for the 3′T dimer proton is striking in that it does not stand out from its neighbors: T_6 and its 3′ neighbors T_{14} and T_8 exchange relatively slowly, not exceeding 35 s^{-1} even at the highest concentrations of catalyst. Indeed, T_{14} and T_8 exchange the most slowly, with comparable rates in both parent and dimer duplexes.

Using eq 3, we can fit straight lines to these data and determine the equilibrium constants for opening each base pair (K_{op}) from the slopes. The values of K_{op} for each base pair are shown in Figure 7 with the bases arranged in order of their occurrence in the sequence. In the case of the parent duplex, there is a gradual decrease in the equilibrium constant for opening, i.e., an increase in base pair stability, from the ends of the duplex to the middle. The equilibrium constants mean that 1/150,000 of the penultimate G_2-C_{19} and G_9-C_{12} base pairs are open at a given time, and the central T_5-A_{16} base pair is 10 times less likely to be open. In contrast, the base pair opening equilibrium constants get larger toward the center of the dimer-containing duplex. The 5′ thymine of the dimer (T_5) has the highest equilibrium constant in the dimer duplex, between 10 and 15 times higher than any other thymine. An equilibrium

dx.doi.org/10.1021/bi401312r | *Biochemistry* 2013, 52, 9275–9285

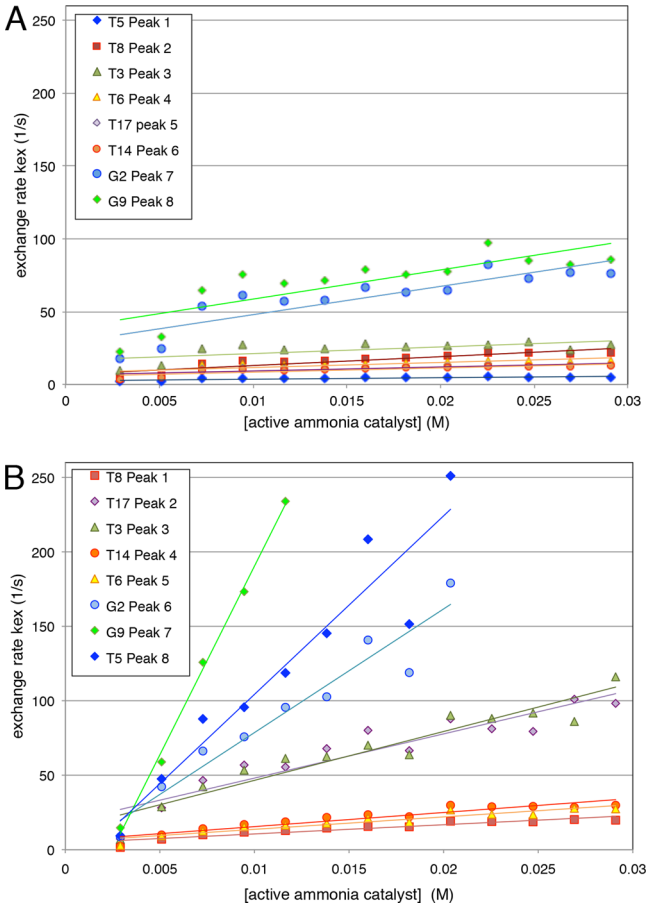

Figure 6. Proton exchange rates (k_{ex}) as a function of ammonia catalyst concentration. For both the parent (A) and dimer (B) duplexes, the rate of exchange increases as the concentration of ammonia catalyst increases for all of the imino protons. Each imino proton is coded in matching colors and shapes between panels for ease of comparison. A fit of these data to eq 3 gives the base pair opening equilibrium constant K_{op}.

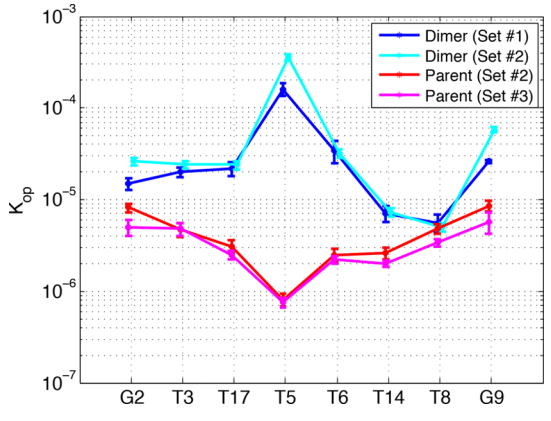

Figure 7. Base pair opening equilibrium constant (K_{op}). K_{op} is shown for each internal base pair in the parent duplex **3**–**4** in the order in which each appears in the sequence. Two independent sample sets are shown for each duplex, measured at the concentrations given in the Methods section. K_{op} values shown here are based upon a pK_a for the thymine imino proton of 10.7; higher pK_a values for the nonaromatic thymine dimer residues would lead to even larger values of K_{op} for T_5 and/or T_6.

constant of 2×10^{-4} corresponds to a ratio of 1:5000 open T_5-A_{16} pairs to closed pairs, a dramatic change from the normal duplex. The 3′ thymine of the dimer (T_6) has an equilibrium constant about ten times lower than the 5′ thymine, 3×10^{-5}. The opening equilibrium constants of the thymines in the 5′ half of the duplex (T_{17}/T_3) are also increased in the presence of the lesion, but the thymines in the 3′ half of the duplex (T_{14} and T_8) have equilibrium constants more similar to those in the normal duplex.

Critically, eqs 3 and 4 include a rate constant for base catalysis k_B that incorporates the difference in pK_a between the DNA base and a base catalyst. Because the dimerization causes a loss of aromaticity of the thymine bases, the imino protons are expected to have a higher pK_a than normal thymine protons (vide infra), and the dimer should be harder to deprotonate than normal thymines. As a result, the difference between the K_{op} values of the dimer thymines and the undamaged parent thymines is even larger than the difference in k_{ex} values between the two sequences.

To control for possible effects of duplex concentration, buffer contaminants, instrumental drift, experimental technique, or other potential errors, the entire titration was repeated multiple times over several years for both sets of duplexes. Two independent data sets measured on different samples are shown in Figure 7 for parent and dimer, clearly illustrating that, although individual spectra may vary, the values of K_{op} are highly reproducible and are independent of duplex concentration.

DISCUSSION

Overall Duplex Stability and Structure with a Thymine Dimer Lesion. To contextualize our imino proton exchange data, we characterized our control "parent" and thymine dimer "lesion" DNA deoxyoligonucleotide duplexes using a variety of techniques. As seen previously for the thymine dimer and other base lesions, the presence of the thymine dimer in this sequence modestly decreases the overall free energy for duplex formation. Here the lesion is enthalpically stabilizing and entropically destabilizing, leading to an overall small loss in ΔG (Figure 1B). Given the weakening of hydrogen bonding and aromatic stacking around the lesion site, enthalpic stabilization is somewhat surprising, pointing to subtle effects of bound water molecules and ions. Enthalpic stabilization and entropic destabilization caused by the lesion has been seen previously for thymine dimers in shorter sequences;[30−32] in contrast, both we and McAteer et al. reported a loss in both enthalpic and entropic stability for thymine dimer lesions in longer DNA duplexes,[12,33] indicating that length and flanking sequence are likely to have yet-unexplored effects on the stability of DNA around the thymine dimer.[34] The enthalpically stabilizing/entropically destabilizing effect of the dimer lesion is not a feature generally shared by base lesions.[24,35−37] However, like many other lesions, the enthalpic and entropic effects tend to compensate for each other, leading to an overall modest change in free energy. [38] As demonstrated elegantly by the Breslauer group, structure and energetics need not relate directly, and a modest change in the free energy of overall duplex formation might correspond to a large structural change or localized disturbances counterbalanced by the plasticity of the DNA structure.[39]

The ultraviolet CD spectrum of dimer-containing DNA is significantly different from the undamaged parent DNA, in both ss and dsDNA (Figure 1C). Our spectra are strongly

dx.doi.org/10.1021/bi401312r | Biochemistry 2013, 52, 9275−9285

reminiscent of the CD spectra of UV-irradiated long genomic DNA published in the 1970s, even though the latter potentially contained a broad selection of lesions and sequence contexts.[40−42] The large spectral changes caused by the lesion are distinctly different, both in magnitude and in sign, from what is observed on the formation of 8-oxoguanine, ethenocytosine, or propanoguanosine lesions; these other base lesions maintain or subtly decrease the magnitude of the 275 and 250 nm bands.[35,38,39] The spectrum of the thymine dimer lesion DNA bears a stronger resemblance to spectra of DNA containing cis-platin, a strongly distorting cross-link that locks DNA into a highly bent shape.[43,44] Based on the spectra, the changes introduced into the DNA duplex by the thymine dimer lesion appear to be significant, though the theory involved in deconvoluting the spectra is quite complex.[45] The intensity and λ_{max} of the broad π to π^*/n to π^* band around 275 nm largely reflect stacking interactions of the aromatic bases.[46] Shifts in this part of the spectrum are consistent with the general principle that two stacked aromatic bases are converted to a new chiral, locked configuration, bending or kinking the DNA but maintaining a largely B-form conformation in the rest of the duplex.

We also used 2D NOESY NMR to establish the integrity of the duplex containing the thymine dimer lesion (Figures 2, 3, SI Figures 2−11). Consistent with the NMR experiments of J.-S. Taylor and colleagues for this sequence[30] and a dimer-containing dodecamer,[12] the integrity of the H1′-H6/H8 NOE walk is largely maintained except on strand 3 at the lesion itself, where the backbone is distorted or the H_6 thymine base resonances shifted upfield under the water resonance. The NOE walk on the complementary strand is maintained intact past the dimer, confirming that the lesion duplex is largely B-form. In addition to electronic changes to the dimer itself, modest changes in chemical shift were observed not only for the flanking and complementary bases, but also for other adenine and thymine protons on the duplex, consistent with perturbations in structure beyond the dimer itself.

Imino Proton Reporters of Individual Base Pair Stability. Because the imino protons of thymine and guanine are involved in base pairing and their proton resonances are found downfield from all other DNA protons, they provide convenient handles for studying DNA base pairing stability by NMR. The imino proton on the 5′ thymine of the dimer (T_5) is shifted significantly upfield from one end of the imino region to the other, consistent with the behavior of the 5′ thymine proton in other sequences.[12,32,47] This change in chemical shift is consistent with the loss of aromaticity in the dimer, and is mirrored by a similar upfield shift in the methyl proton on this base. The dimer 3′ thymine's (T_6) imino proton does not change nearly as dramatically, nor does its methyl proton, even though this base also loses its aromatic character. Previous investigators pointed to weaker hydrogen bonding at the 5′ T imino as being responsible for the difference in chemical shift. Indeed the two are likely correlated, though it is less clear that weaker hydrogen bonding need be the *cause* of the upshift instead of another marker of electronic perturbations to the 5′ dimer thymine.[12,32] Taylor and colleagues compared the chemical shifts between normal thymine and dimer dinucleobase model compounds in $CHCl_3$, concluding that hydrogen bonding could not fully explain the chemical shifts. Ring shielding is likely to affect the imino proton chemical shift because the dimer bases project out toward their flanking adenines more than aromatic, well-stacked thymines, pushing the imino protons (particularly on the 5′ thymine) closer to the π clouds of their flanking adenines.[12,48−52]

In addition, the asymmetry in chemical shift between the 5′ and 3′ thymine imino protons may reflect asymmetries in the electron distribution across the dimer that are masked or compounded by the magnetic anisotropy effects inherent to the spectroscopic method. Using ab initio SCF calculations, Aida et al. demonstrated that the puckering of the cyclobutane ring causes notable differences in the electronic structure of the two bases such that the density of the HOMO orbital is skewed preferentially toward one ring.[53] Using ab initio MO calculations, Sugiyama and Saito demonstrated that electronic interactions between stacked bases in the core of duplex DNA substantially perturb the ionization potential and other electronic properties of individual guanines such that otherwise identical guanines become quite distinct from one another.[54] In a similar vein, the asymmetry in chemical shift of the thymine dimer in duplex DNA, not observed in dinucleotide model compounds,[12] nor many computational studies of model dimer dinucleobases, may point to an unequal electronic distribution between the 5′ and 3′ dimer thymines that is intimately tied to its base stacking environment in dsDNA.

A series of temperature-dependent 1D ^{1}H spectra demonstrate that, for both parent and dimer duplexes, all of the imino protons are visible below room temperature except for those on the terminal guanines G_{11} and G_{20} (Figure 4). The T_5 and T_6 dimer proton resonances are both visible, confirming that qualitatively base pairing is conserved at the lesion. Direct measurement of imino exchange times was achieved via magnetization transfer from water protons as described by Guéron and Leroy (Figure 5).[23] It is apparent from the raw spectra that the protons in the dimer duplex exchange robustly with water; in particular, the penultimate guanines G_2 and G_9 and the 5′ dimer proton T_5 exchange the most rapidly and thoroughly with solvent.

Since the base pairs can reclose without exchange, increasing the concentration of ammonia base catalyst increases the rate of proton exchange in a linear fashion at low concentrations (Figure 6), allowing us to determine via eq 3 the equilibrium constant for opening of each base pair K_{op} (Figure 7). Though the rates of base pair opening and closing cannot not be directly measured at low to moderate catalyst concentrations, the increased equilibrium constants mean that either (1) the rate of opening must be faster at the dimer, (2) the rate of closing must be slower, or (3) both. Thus, these equilibrium constant measurements dramatically illustrate that the dynamic motions of the base pairs in the dimer duplex are significantly different than in the parent duplex, favoring an open state of undetermined geometry (vide infra) more often than do normal thymines.[24] Also, the measurements of base pair opening are independent of the duplex-single strand equilibrium, since they are not affected by DNA concentration (Figure 7). Thus, the decrease in duplex stability probed by the thermodynamic experiments (Figure 1) is not directly responsible for the differences in K_{op} between the parent and dimer duplexes.

The patterns in base pair opening are consistent with the X-ray and NMR crystal structures, while expanding upon these static pictures. Most notably, the base pair opening equilibrium constant of the T_5-A_{16} pair (5′ thymine of the dimer) is one hundred times larger than K_{op} for the same base pair in the parent duplex. The X-ray crystal and NMR structures of thymine dimers show a long, weak bond between the 5′T and

its complement, though in both cases the adenine N6-to-thymine O4 hydrogen bond is longer, weaker, and less optimally aligned than the imino proton hydrogen bond. The method of Guéron and colleagues assumes that the imino proton is not available for exchange until the base pair is "open" and somewhat available to solvent, therefore modeling base pair opening and not just imino proton exchange.[23] As a result our measured equilibrium constant more strongly favoring the open state is qualitiatively consistent with the proposed ~1.5 hydrogen bonds between the 5′ thymine and adenine, even if the imino proton hydrogen bond is actually the stronger of the two. Both published structures show normal base pairing for the 3′ thymine and flanking bases. By direct measurement of exchange rates, we have determined that the K_{op} for the 3′ thymine of the dimer and the 5′ flanking base pair (T_{17}/A_4) are in fact ten times larger than in the parent. The T_3-A_{18} pair on the 5′ side of the dimer may also be weakened somewhat. In contrast the base pairs on the 3′ side of the dimer are relatively normal within error, giving us a picture of a duplex that is asymmetrically destabilized. This asymmetry in base pair stability is reminiscent of the crystal structure in which the twisting and tilt angles are perturbed flanking the dimer on the 5′ but not the 3′ side. Also, we previously demonstrated that the mismatch-specific photocleavage agent $Rh(bpy)_2(chrysi)^{3+}$ selectively binds dimer-containing DNA immediately 5′ to the thymine dimer, consistent with the idea that base pair opening is increased asymmetrically near the lesion.[33]

It is important to note that the values of K_{op} presented in Figure 7 are based upon the approximation that both thymine dimer imino proton pK_a's are 1 pH unit higher than that of normal thymidine as measured in a dinucleobase model system.[29] Formation of the thymine dimer involves a loss of aromaticity that should increase the pK_a of both imino protons, and the upfield-shifted resonance of the 3′ T imino proton is consistent with a modestly increased pK_a.[55] A longer T-A base pairing distance in the crystal structure,[11] significantly upfield-shifted imino resonances (here and ref 12) and increased $^{15}N-^{1}H$ coupling constants[55,56] all support a more substantially increased pK_a for the 5′ T of the dimer in DNA, consistent with an unequal electron distribution between dimer thymines when stacked within DNA discussed above. If the pK_a of the T_5 proton is 11.7 instead of 10.7, the K_{op} increases by approximately ten times to become $\sim 2.5 \times 10^{-3}$. Consequently, the values of K_{op} for T_5 and T_6 presented in Figure 7 represent a lower bound, and in fact the equilibrium constants might favor the open state at the 5′ T more than is shown.

Because the structures of many DNA repair enzymes including photolyase require a lesion to be flipped out into the protein active site, the question arises as to the role of spontaneous extrusion in the localization and binding of a lesion. The thymine dimer's repair proteins may capture a dynamic, exposed lesion in the act of breathing. These measurements stand in sharp contrast to our observations of the 8-oxoguanine lesion, which does not significantly perturb base pair opening in its vicinity.[24] Recognition and extrusion of the 8-oxoguanine lesion by its repair proteins may require active perturbation of the DNA and probing by the enzyme.[57] However, they raise the important issue of what it means for the thymine dimer to be more labile at the 5′ thymine than the 3′ thymine. The 5′ thymine cannot rotate from the core of the duplex without its locked 3′ thymine; the 10-fold difference in K_{op} values between the 5′ and 3′ thymines hints that when the dimer base pairs open spontaneously, it is likely to be the complementary adenines that destack and open to solution. Spontaneous flipping of the complementary adenines has emerged from some molecular dynamics simulations[58] but not others.[16] Notably, complementary adenine flipping at the 5′T/3′A site has been seen in the structure of T4 endo V binding to a thymine dimer DNA.[14] In a recent co-crystal structure with DNA containing a 6–4 photoproduct, the UV damage endonuclease UVDE is seen to flip the lesion out into an active site pocket while also capturing the complementary adenines extrahelically in a second pocket.[59] This pyrimidine-specific damage endonuclease likely binds the *cis-syn* dimer lesion in a similar fashion. Due to the increase in base pair opening, the cellular repair machineries may have evolved to recognize the solvent-exposed adenines opposite a thymine dimer lesion in addition to the lesion itself.

Regardless of which base spontaneously flips into solution, the presence of a more dynamic, open 5′T-A pair is likely to increase bending and flexibility at the dimer site, facilitate binding of the dimer in the active site of photolyase and other repair enzymes, and potentially serve as a recognition element in genome-wide repair.

■ ASSOCIATED CONTENT

Supporting Information

Melting temperature curves, structures of normal base pairs and the thymine dimer lesion, annotated 2D NOESY spectra for parent and lesion duplexes, and tables of thermodynamic and chemical shift data. This material is available free of charge via the Internet at http://pubs.acs.org..

■ AUTHOR INFORMATION

Corresponding Author

*Telephone: (781) 283-3028; Fax: (781) 283-3642; e-mail: mnunez@wellesley.edu.

Funding

This work was supported by the Camille and Henry Dreyfus Foundation, the Clare Boothe Luce Foundation, the Radcliffe Institute for Advanced Study at Harvard University, the National Institutes of Health/NIGMS (1R15GM083250), and the National Science Foundation (CHE-0922804).

Notes

The authors declare no competing financial interest.

■ ACKNOWLEDGMENTS

Our deepest and most heartfelt thanks go to our NMR guru Dr. Charles Dickinson, without whom these experiments would not be possible. We would also like to thank Drs. Cristina Suarez, Haribabu Arthanari, and Lila Gierasch for their assistance with this work.

■ ABBREVIATIONS

CD, circular dichroism spectropolarimetry; NOESY, Nuclear Overhauser effect spectroscopy; HPLC, high performance liquid chromatography; DSS, 4,4-dimethyl-4-silapentane-1-sulfonic acid; k_{ex}, rate of imino proton exchange; K_{op}, equilibrium constant for base pair opening

■ REFERENCES

(1) Friedberg, E. C., Walker, G. C., Siede, W., Wood, R. D., Schultz, R. A., and Ellenberger, T. (2006) DNA Repair and Mutagenesis, 2nd ed, ASM Press, Washington, DC.

(2) Smith, C. A., Baeten, J., and Taylor, J.-S. (1998) The ability of a variety of polymerases to synthesize past site-specific *cis-syn*, *trans-syn*-II, (6−4), and Dewar photoproducts of thymidylyl-(3′->5′)-thymidine. *J. Biol. Chem. 273*, 21933−21940.
(3) Selby, C., Drapkin, R., Reinberg, D., and Sancar, A. (1997) RNA polymerase II stalled at a thymine dimer: footprint and effect on excision repair. *Nucleic Acids Res.*, 787−793.
(4) Brueckner, F., Hennecke, U., Carell, T., and Cramer, P. (2007) CPD damage recognition by transcribing RNA polymerase II. *Science 315*, 859−862.
(5) McCulloch, S., Kokoska, R., Masutani, C., Iwai, S., Hanaoka, F., and Kunkel, T. (2004) Preferential *cis-syn* thymine dimer bypass by DNA polymerase η occurs with biased fidelity. *Nature 428*, 97−100.
(6) Johnson, R. E., Prakash, S., and Prakash, L. (1999) Efficient bypass of a thymine-thymine dimer by yeast DNA polymerase, Pol η. *Science 283*, 1001−1004.
(7) Sancar, A., and Mu, D. (1997) Model for XPC-independent transcription-coupled repair of pyrimidine dimers in humans. *J. Biol. Chem. 272*, 7570−7573.
(8) Svejstrup, J. Q. (2002) Mechanisms of transcription-coupled DNA repair. *Nat. Rev. Mol. Cell Biol. 3*, 21−29.
(9) Husain, I., Griffith, J., and Sancar, A. (1988) Thymine dimers bend DNA. *Proc. Natl. Acad. Sci. U.S.A. 85*, 2558−2562.
(10) Wang, C.-I., and Taylor, J.-S. (1991) Site-specific effect of thymine dimer formation on dAn•dTn tract bending and its biological implications. *Proc. Natl. Acad. Sci. U.S.A. 88*, 9072−9076.
(11) Park, H., Zhang, K., Ren, Y., Nadji, S., Sinha, N., Taylor, J.-S., and Kang, C. (2002) Crystal structure of a DNA decamer containing a *cis-syn* thymine dimer. *Proc. Natl. Acad. Sci. U.S.A. 99*, 15965−15970.
(12) McAteer, K., Jing, Y., Kao, J., Taylor, J.-S., and Kennedy, M. A. (1998) Solution-state structure of a DNA dodecamer duplex containing a *cis-syn* thymine cyclobutane dimer, the major UV photoproduct of DNA. *J. Mol. Biol. 282*, 1013−1032.
(13) Mees, A., Klar, T., Gnau, P., Hennecke, U., Eker, A., Carell, T., and Essen, L. (2004) Crystal structure of a photolyase bound to a CPD-like DNA lesion after *in situ* repair. *Science 306*, 1789−1793.
(14) Vassylyev, D., Kashiwagi, T., Mikami, Y., Ariyoshi, M., Iwai, S., Ohtsuka, E., and Morikawa, K. (2004) Atomic model of a pyrimidine dimer excision repair enzyme complexed with a DNA substrate: structural basis for damaged base recognition. *Cell 1995*, 1−10.
(15) Lukin, M., and de los Santos, C. (2006) NMR structures of damaged DNA. *Chem. Rev. 106*, 607−686.
(16) O'Neil, L. L., Grossfield, A., and Wiest, O. (2007) Base flipping of the thymine dimer in duplex DNA. *J. Chem. Phys. B 111*, 11843−11849.
(17) Wilson, T. J., Crystal, M. A., Rohrbaugh, M. C., Sokolowsky, K. P., and Gindt, Y. M. (2011) Evidence from thermodynamics that DNA photolyase recognizes a solvent-exposed CPD lesion. *J. Phys. Chem. B 115*, 13746−13754.
(18) Goddard, T. D., and Kneller, D. G. *Sparky 3*, University of California, San Francisco.
(19) Hare, D., Wemmer, D., Chou, S., Drobny, G., and Reid, B. (1983) Assignment of the non-exchangeable resonances of d-(CGCGAATTCGCG) using two-dimensional nuclear magnetic resonance methods. *J. Mol. Biol. 171*, 319−336.
(20) Scheek, R. M., Russo, N., Boelens, R., Kaptein, R., and van Boom, J. H. (1983) Sequential resonance assignments in DNA proton NMR spectra by two-dimensional NOE spectroscopy. *J. Am. Chem. Soc. 105*, 2914−2916.
(21) Wemmer, D. Structure and dynamics by NMR, in *Nucleic Acids: Structures, Properties, and Functions* (Bloomfield, V., Crothers, D. M., and Tinoco, I., Eds.) University Science Books, Sausalito, CA.
(22) Macke, T. J., and Case, D. A. (1998) Modeling of unusual nucleic acid structures, in *Molecular Modeling of Nucleic Acids* (Leontis, N. B., and SantaLucia, J., Jr, Eds.) pp 379−393, American Chemical Society, Washington, D.C.
(23) Guéron, M., and Leroy, J. (1995) Studies of base pair kinetics by NMR measurement of proton exchange. *Meth. Enzymol. 261*, 383−413.
(24) Crenshaw, C. M., Wade, J. E., Arthanari, H., Frueh, D., Lane, B. F., and Núñez, M. E. (2011) Hidden in plain sight: subtle effects of the 8-oxoguanine lesion on the structure, dynamics, and thermodynamics of a 15-base pair oligodeoxynucleotide duplex. *Biochemistry 50*, 8463−8477.
(25) Raiford, D., Fisk, C., and Becker, E. (1979) Calibration of methanol and ethylene glycol nuclear magnetic resonance thermometers. *Anal. Chem. 51*, 2050−2051.
(26) Delaglio, F., Grzesiek, S., Vuister, G. W., Zhu, G., Pfeifer, J., and Bax, A. (1995) NMRPipe: a multidimensional spectral processing system based on UNIX pipes. *J. Biomol. NMR 6*, 277−293.
(27) Every, A. E., and Russu, I. M. (2008) Influence of magnesium ions on spontaneous opening of DNA base pairs. *J. Phys. Chem. B 112*, 7689−7695.
(28) Guéron, M., Charretier, E., Hagerhorst, J., Kochoyan, M., Leroy, J., and Moraillon, A. (1990) Applications of imino proton exchange to nucleic acid kinetics and structures, in *Structure and Methods Vol. 3: DNA & RNA*, Proceedings of the Sixth Conversation in the Discipline of Biomolecular Stereodynamics Held at the State University of New York at Albany, June 6−10, 1989 (Sarma, R. H., and Sarma, M. H., Eds.) Adenine Press, Schenectady, NY.
(29) Herbert, M., LeBlanc, J., Weinblum, D., and Johns, H. (1969) Properties of thymine dimers. *Photochem. Photobiol. 9*, 33−43.
(30) Taylor, J.-S., Garrett, D. S., Brockie, I. R., Svoboda, D. L., and Telser, J. (1990) ^{1}H NMR assignment and melting temperature study of *cis-syn* and *trans-syn* thymine dimer containing duplexes of d(CGTATTATGC)• d(GCATAATACG). *Biochemistry 29*, 8858−8866.
(31) Frankel, E. (2011) Elucidating the dynamic properties of *cis-syn* thymine dimer lesion-containing DNA using thermodynamic techniques. Mount Holyoke College senior honors thesis.
(32) Kemmink, J., Boelens, R., Koning, T., van der Marel, G. A., van Boom, J. H., and Kaptein, R. ^{1}H NMR study of the exchangeable protons of the duplex d(GCGT<>TGCG) •d(CGCAACGC) containing a thymine photodimer. *Nucleic Acids Res. 15*, 4645−4653.
(33) Rumora, A. E., Kolodziejczak, K. M., Malhowski Wagner, A., and Núñez, M. E. (2008) Thymine dimer-induced structural changes to the DNA duplex examined with reactive probes. *Biochemistry 47*, 13026−13035.
(34) Gelfand, C. A., Plum, G. E., Grollman, A. P., Johnson, F., and Breslauer, K. J. (1998) Thermodynamic consequences of an abasic lesion in duplex DNA are strongly dependent on base sequence. *Biochemistry 37*, 7321−7327.
(35) Chinyengetere, F., and Jamieson, E. R. (2008) Impact of the oxidized guanine lesion spiroiminodihydantoin on the conformation and thermodynamic stability of a 15-mer DNA duplex. *Biochemistry 47*, 2584−2591.
(36) Plum, G. E., Grollman, A. P., Johnson, F., and Breslauer, K. J. (1992) Influence of an exocyclic guanine adduct on the thermal stability, conformation, and melting thermodynamics of a DNA duplex. *Biochemistry 31*, 12096−12102.
(37) Sági, J., Perry, A., Hang, B., and Singer, B. (2000) Differential stabilization of the DNA oligonucleotide double helix by a T-G mismatch, 3,N4-ethenocytosine, 3,N4 ethanocytosine, or an 8-(hydroxymethyl),3,N4-ethenocytosine adduct incorporated into the same sequence contexts. *Chem. Res. Toxicol. 13*, 839−845.
(38) Gelfand, C., Plum, G., Grollman, A., Johnson, F., and Breslauer, K. (1998) The impact of an exocyclic cytosine adduct on DNA duplex properties: significant thermodynamic consequences despite modest lesion-induced structural alterations. *Biochemistry 37*, 12507−12512.
(39) Plum, G., and Breslauer, K. (1994) DNA lesions: a thermodynamic perspective. *Ann. N.Y. Acad. Sci. 726*, 45−56.
(40) Vorlickova, M., and Palecek, E. (1974) A study of changes in DNA conformation caused by ionizing and ultra-violet radiation by means of pulse polarography and circular dichroism. *Int. J. Radiat. Biol. Relat. Stud. Phys. Chem. Med. 26*, 363−372.
(41) Lang, H. (1975) CD studies of conformational changes of DNA upon photosensitized UV-irradiation at 313 nm. *Nucleic Acids Res. 2*, 179−183.

(42) Toulmé, J. J., and Hélène, C. (1977) Specific recognition of single-stranded nucleic acids. Interaction of tryptophan-containing peptides with native, denatured, and ultraviolet-irradiated DNA. *J. Biol. Chem. 252*, 244−249.
(43) Poklar, N., Pilch, D. S., Lippard, S. J., Redding, E. A., Dunham, S. U., and Breslauer, K. J. (1996) Influence of cisplatin intrastrand crosslinking on the conformation, thermal stability, and energetics of a 20-mer DNA duplex. *Proc. Natl. Acad. Sci. U.S.A. 93*, 7606−7611.
(44) Pilch, D. S., Dunham, S. U., Jamieson, E. R., Lippard, S. J., and Breslauer, K. J. (2000) DNA sequence context modulates the impact of a cisplatin 1, 2-d (GpG) intrastrand cross-link on the conformational and thermodynamic properties of duplex DNA. *J. Mol. Biol. 296*, 803−812.
(45) Kypr, J., Kejnovska, I., Renciuk, D., and Vorlickova, M. (2009) Circular dichroism and conformational polymorphism of DNA. *Nucleic Acids Res. 37*, 1713−1725.
(46) Bush, C. A. (1974) Ultraviolet spectroscopy, circular dichroism, and optical rotatory dispersion. *Basic Principles in Nucleic Acid Chemistry 2*, 91−169.
(47) Kim, J.-K., Patel, D., and Choi, B.-S. (1995) Contrasting structural impacts induced by cis-syn cyclobuane dimer and (6−4) adduct in DNA duplex decamers: implication in mutagenesis and repair activity. *Photochem. Photobiol. 62*, 44−50.
(48) Patel, D., and Tonelli, A. E. (1974) Proton Nuclear Magnetic Resonance investigations and ring current calculations of Guanine N-1 and Thymine N-3 hydrogen bonded protons in double-helical deoxyribonucleotides in aqueous solution. *Proc. Natl. Acad. Sci. U.S.A. 71*, 1945−1948.
(49) Arter, D. B., and Schmidt, P. G. (1976) Ring current shielding effects in nucleic acid double helices. *Nucleic Acids Res. 3*, 1437−1447.
(50) Moyna, G., Zauhar, R., Williams, H., Nachman, R. J., and Scott, A. I. (1998) Comparison of ring current methods for use in molecular modeling refinement of NMR derived three-dimensional structures. *J. Chem. Inf. Comput. Sci. 38*, 702−709.
(51) Case, D. A. (1995) Calibration of ring current effects in proteins and nucleic acids. *J Biomol. NMR 6*, 341−346.
(52) Giessner-Prettre, C., and Pullman, B. (1976) Ring-current effects in the NMR of nucleic acids: a graphical approach. *Biopolymers 15*, 2277−2286.
(53) Aida, M., Kaneko, M., and Dupuis, M. (1996) An *ab initio* MO study on the thymine dimer and its radical cation. *Int. J. Quantum Chem. 57*, 949−957.
(54) Sugiyama, H., and Saito, I. (1996) Theoretical studies of GG-specific photocleavage of DNA via electron transfer: significant lowering of ionization potential and 5′-localization of HOMO of stacked GG bases in B-form DNA. *J. Am. Chem. Soc. 118*, 7063−7068.
(55) Ishikawa, R., Ono, A., and Kainosho, M. (2003) The NMR studies of substituent effects on the NH-N hydrogen bond in duplex DNA using 2′-deoxynebularine and ^{15}N labeled 5-substituted 2′-deoxyuridine base pairs. *Nucleic Acids Res. Suppl. 3*, 57−58.
(56) Bdour, H. M., Kao, J. L.-F., and Taylor, J.-S. (2006) Synthesis and characterization of a [3-^{15}N]-labeled *cis-syn* thymine dimer-containing DNA duplex. *J. Org. Chem. 71*, 1640−1646.
(57) David, S. S., O'Shea, V. L., and Kundu, S. (2007) Base-excision repair of oxidative DNA damage. *Nature 447*, 941−950.
(58) Yamaguchi, H., van Aalten, D., Pinak, M., Furukawa, A., and Osman, R. (1998) Essential dynamics of DNA containing a *cis-syn* cyclobutane thymine dimer lesion. *Nucleic Acids Res. 26*, 1939−1946.
(59) Meulenbroek, E. M., Peron Cane, C., Jala, I., Iwai, S., Moolenaar, G. F., Goosen, N., and Pannu, N. S. (2013) UV damage endonuclease employs a novel dual-dinucleotide flipping mechanism to recognize different DNA lesions. *Nucleic Acids Res. 41*, 1363−1371.